Relationship Between El Niño-Southern Oscillation and Atmospheric Aerosols in the Legal Amazon

Augusto G. C. Pereira *, Rafael Palácios *, Paula C. R. Santos, Raimundo Vitor S. Pereira, Glauber Cirino, Breno Imbiriba

Posted Date: 1 October 2023

doi: 10.20944/preprints202310.0017.v1

Keywords: Aerosol; ENSO; Black Carbon; Remote Sensing; Amazon

Article

Relationship between El Niño-Southern Oscillation and Atmospheric Aerosols in the Legal Amazon

Augusto G. C. Pereira [1,*], Rafael Palácios [1,*], Paula C. R. Santos [2], Raimundo Vitor S. Pereira [1], Glauber Cirino [1] and Breno Imbiriba [1]

[1] Institute of Geosciences, Federal University of Pará, UFPA, Belém 66075-110, PA, Brazil; vitorspereira2010@gmail.com (R.V.S.P.); glaubercirino@ufpa.br (G.C.); brenoimbiriba@gmail.com (B.I.)

[2] Institute of Biologicalf Sciences, Federal University of Pará, UFPA, Belém 66075-110, PA, Brazil; paulacarolina954@gmail.com.

* Correspondence: costapereira620@gmail.com; Tel.: +5591999088462, (A.G.C.P); rafaelpgfa@gmail.com; Tel.: +5511998488650, (R.P.).

Abstract: The El Niño-Southern Oscillation (ENSO) stands as the paramount tropical phenomenon of climatic magnitude resulting from ocean-atmosphere interaction. Due to its atmospheric teleconnection mechanism, ENSO wields influence over diverse environmental variables spanning distinct atmospheric scales, thereby potentially impacting the spatiotemporal distribution of atmospheric aerosols. Within this framework, this study aims to appraise the relationship between ENSO and atmospheric aerosols across the Legal Amazon during the period between 2006 and 2011. Over this quinquennium, four ENSO events were identified. Concurrently, an analysis was conducted on the spatiotemporal variability of aerosol optical depth (AOD) and AOD extinction for Black Carbon (EAOD-BC), concomitant with said ENSO events, utilizing data derived from the Aerosol Robotic Network (AERONET), MERRA-2 model, and ERSSTV5. Through the Windowed Cross Correlation (WCC) approach, statistically significant phase lags of up to 4 to 6 months were observed between ENSO indicators and atmospheric aerosols. Moreover, conspicuous increases of over 100% in atmospheric aerosol concentration were evidenced subsequent to El Niño periods, especially during the intervals encompassing the La Niña phase, particularly within the La Niña CP (Central Pacific)/Modoki category. By analyzing specific humidity anomalies (QA), exceptional scenarios in the region were detectable. This observation suggests a notable singularity when juxtaposed with antecedent investigations and typical average patterns characterizing the impacts on the Amazonian region.

Keywords: aerosol; ENSO; black carbon; remote sensing; amazon

1. Introduction

The El Niño-Southern Oscillation (ENSO), in its distinct phases, exerts various modulations on climate due to its atmospheric teleconnection mechanism in the Amazon region [1]. This biome, encompassing 40% of the world's tropical forests [2], is particularly sensitive to the influences of ENSO. Recent studies, such as that by Li et al. [3], demonstrate that climate variations modulated by ENSO can have substantial impacts on atmospheric particles. Additionally, Zhou et al. [4] present two significant perspectives. Firstly, they argue that aerosol emissions resulting from Amazonian fires may interfere with both the intensity and duration of ENSO. Secondly, the study suggests that ENSO might influence the spatial distribution of aerosol emissions originating from Amazonian fires through extreme climatic events, such as severe droughts, potentially leading to outbreaks of fires [5], directly impacting the Amazonian biome [6]. Evaluating aerosol distributions over the Amazon has been increasingly studied, primarily due to their contributions from biomass burning, as in the works of Alves et al.[7] and Holanda et al. [8,9]. However, investigating the primary hypothesis regarding the relationships with ENSO remains underexplored for the region.

The determination of aerosols is of paramount importance, representing a topic that has gained increasing prominence in research. One of these aerosols of particular significance is Black Carbon (BC), recognized for its unique physical properties. This compound exhibits a strong capacity for

 doi:10.20944/preprints202310.0017.v1

solar radiation absorption within the visible and infrared electromagnetic spectrum [10], constituting the most important light-absorbing aerosol in the atmosphere with respect to global warming [11]. BC originates from both incomplete biomass combustion and incomplete fossil fuel burning [12], being emitted both naturally and anthropogenically.

Recent studies, such as those conducted by Holanda et al. [8,9], investigate the impact of long-range transport on aerosol estimates in the Amazon region, with emphasis on BC. The Amazon is subject not only to the influence of fires originating within the biome itself and surrounding areas but is also substantially affected by transatlantic transport from Africa, including smoke, dust, and other particles [9,13]. Lou et al. [14] highlighted the relationship between ENSO and BC emissions in specific regions, resulting in an increase in the frequency of extreme ENSO events, mediated by a series of factors. Among these, the increase in BC emissions from the northern hemisphere stands out, with the potential to attenuate thermal gradients between distinct latitudes and facilitate heat transfer towards the North Pole. Furthermore, such emissions can lead to decreased energy dispersion in the tropics, consequently intensifying the increase in sea surface temperature (SST). The combination of these elements demonstrates the significant contribution of BC to the increase in the incidence of extreme events associated with ENSO. The study by Kim et al. [15] suggests that La Niña shows a direct association with increased aerosol concentrations in specific regions. This association finds part of its explanation in the moisture transport process, upper tropospheric heating, and increased precipitation during specific periods.

The climatic modulation promoted by ENSO significantly influences the spatiotemporal distribution of atmospheric particles in various distinct regions [16,17]. In the Amazon region, the atmosphere is subject to modulations arising from synoptic systems, exemplified by the Intertropical Convergence Zone (ITCZ), whose seasonal variations manifest from north to south. Additionally, seasonal influences from austral summer systems are also observed, including the reduction in aerosol estimates in the Amazon, attributed to the Bolivian High (BH), Upper Tropospheric Cyclonic Vortex (UTCV), and South Atlantic Convergence Zone (SACZ). The region is also subject to influences from mesoscale convective systems [18] throughout most of the year. The combination of these factors results in pronounced seasonality in aerosol concentrations [8], as well as in other properties of these particles [19–21].

Given this perspective, a deeper analysis of the various ways in which climatic drivers, in conjunction with meteorological elements, can impact aerosol concentration estimates in the Amazon region becomes necessary. Therefore, this study aims to evaluate the spatiotemporal relationship between ENSO and atmospheric aerosols over the Legal Amazon, specifically within the period between 2006 and 2011. Within this brief five-year interval, four ENSO events were observed, revealing a remarkable singularity when compared to previous investigations and the characteristic average patterns of effects in the Amazonian region.

Materials and Methods

2.1. ENSO Indicators Data

Interventionary studies involving animals or humans, and other studies that require ethical approval, must list the authority that provided approval and the corresponding ethical approval code.In this study, an analysis of sea surface temperature anomalies (SSTA) was carried out in the central tropical Pacific Ocean (CTPO) region from January 2006 to December 2011 (Table 1). Over these four years, two El Niño and La Niña events were identified, alternating between them. The SSTA was evaluated from the western coast of Peru to the eastern region of Melanesia and the eastern coast of Oceania. It is of utmost importance to meticulously examine ENSO events, as they manifest in two distinct patterns: Modoki/Central Pacific (CP) and Canonical/Eastern Pacific (EP) [22,23].

Preprints (www.preprints.org) | NOT PEER-REVIEWED | Posted: 1 October 2023 doi:10.20944/preprints202310.0017.v1

Table 1. Data from the oceanic component, atmospheric component, and atmospheric aerosols used in the study.

Data	Spatial Resolution	Period	Source	Version	Data Scale
SSTA in Niño 1+2, Niño 3, Niño 3.4 and Niño 4 regions	2º x 2º	Availability: From 1950 - to the present; Climatology: 1971-2000; Utilized in the Study: 2006-2011.	https://psl.noaa.gov/data/climateindices/list/	ERSSTV5	Monthly
SOI	-	Availability: From 1951- to the present; Utilized in the Study: 2006-2011.	https://psl.noaa.gov/data/climateindices/list/	-	Monthly
AOD 500 nm (AERONET)	-	Availability: From 1993-2021 (AF), 2006-2021 (JP) e 2001-2023 (RB); Utilized in the Study: 2006-2011.	https://aeronet.gsfc.nasa.gov/	Nível 2.0	Monthly
AOD 550 nm extinction for Black Carbon (MERRA2)	0.5° x 0.625°	Availability: From 1980 - to the present; Utilized in the Study: 2006-2011	https://disc.gsfc.nasa.gov/datasets?project=MERRA-2	M2TMNXAER v5.12.4	Monthly
Specific Humidity Anomaly at 2m (MERRA-2)	0.5° x 0.625°	Availability: From 1980 - to the present; Climatology: 1980-2020; Utilized in the Study: 2006-2011	https://disc.gsfc.nasa.gov/datasets?project=MERRA-2	M2TMNXSLV v5.12.4	Monthly

Four regions within the CTPO were considered, denoted as Niño 1+2 (80° W – 90° W), 3 (90° W – 150° W), 3.4 (120° W – 170° W), and 4 (150° W – 160° E). The Niño 3.4 region is monitored using an index referred to as the Oceanic Niño Index (ONI). Figure 1 illustrates the geographic delineation of the analyzed regions and the SSTA within each Niño region. Oceanic data for monthly anomalies are derived from the Extended Reconstructed Sea Surface Temperature Version 5 (ERSSTV5) dataset, sourced from in-situ observations provided by the Physical Sciences Laboratory (PSL) of NOAA (https://psl.noaa.gov/data/climateindices/list/).

Preprints (www.preprints.org) | NOT PEER-REVIEWED | Posted: 1 October 2023 doi:10.20944/preprints202310.0017.v1

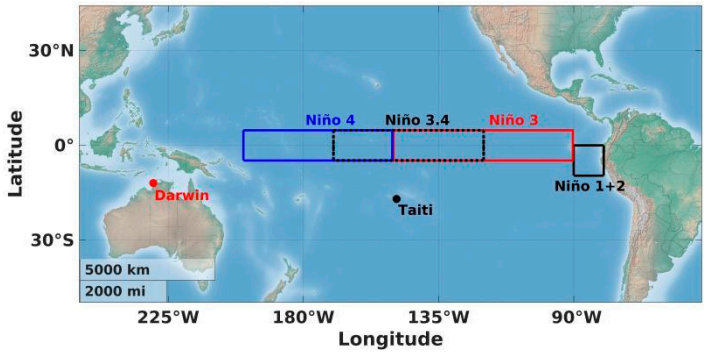

Figure 1. Location of the Niño 1+2, 3, 3.4, and 4 regions in the central Tropical Pacific Ocean, where sea surface temperature anomalies were analyzed. The positions of Tahiti and Darwin, used to derive the Southern Oscillation Index (SOI), are also highlighted.

The monthly Southern Oscillation Index (SOI) is derived from data provided by the NOAA Climate Prediction Center (CPC) and involves the analysis of pressure anomalies in Darwin (12.4° S, 130.9° E) and Tahiti (17.5° S, 149° W) in the Southern Tropical Pacific Ocean (Figure 1). Historical data spanning from January 2006 to December 2011 are encompassed in this study (Table 1), and these data are available online at https://psl.noaa.gov/data/climateindices/list/. During El Niño events (positive ATSM), the SOI exhibits negative values, whereas during La Niña events (negative ATSM), the SOI assumes positive values [24].

2.2. Atmospheric Aerosol Data

2.2.1. AERONET

Remote sensing is used to monitor the optical properties of aerosols, primarily through the ground-based monitoring network known as Aerosol Robotic Networks (AERONET). This network continuously provides data on various aerosol parameters and characteristics on a global and regional scale [25]. The parameter utilized in this study is the Aerosol Optical Depth (AOD), which represents the magnitude index of solar radiation extinction caused by aerosols due to scattering and absorption processes [26,27]. AERONET comprises globally distributed spectral radiometers, and AOD data are classified into levels 1.0, 1.5, and 2.0. Level 1 corresponds to raw measurements, level 1.5 includes processed measurements that eliminate cloud and precipitation interferences, while level 2 undergoes final calibration with local corrections and network quality assurance [25].

The sites located within the Legal Amazon, which were used for the assessment of AOD at 500 nm from level 2.0 data for the period between 2006 and 2011, are derived from Alta Floresta (MT), Ji-Paraná (RO), and Rio Branco (AC) (Table 1). Figure 2 displays the locations of the sites analyzed in this study. These sites are situated in the heart of the Legal Amazon, specifically in the deforestation arc, an area experiencing significant adverse effects from excessive biome exploitation and agricultural expansion.

Preprints (www.preprints.org) | NOT PEER-REVIEWED | Posted: 1 October 2023 doi:10.20944/preprints202310.0017.v1

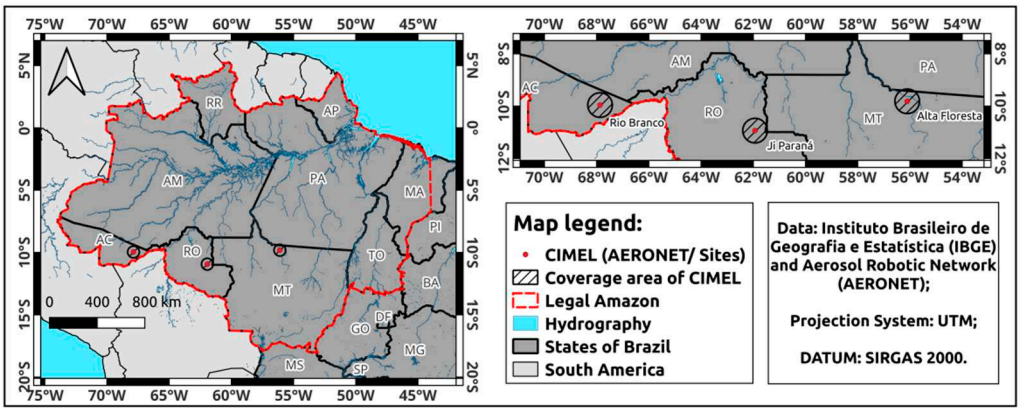

Figure 2. Location of the Legal Amazon for spatial evaluation of EAOD-BC and the sites of AERONET in Alta Floresta (MT), Ji-Paraná (RO), and Rio Branco (AC), over which AOD and EAOD-BC data were analyzed, with the location of the CIMEL solar photometer and its coverage area with a radius of 50 km.

In the processing of AOD data at 500 nm, we utilized measurements of the Extinction Ångström Exponent (EAE) for the spectral range of 440-870 nm. The EAE provides the spectral dependence of AOD and enables the conversion of AOD at 500 nm to other spectral ranges. Point measurements of AOD at 500 nm and AE from AERONET were employed to calculate daily averages. The AE was used to interpolate AOD from AERONET at 550 nm in accordance with Equation 1:

$$AOD\ 550\ nm\ = AOD\ 500\ nm\ \left(\frac{550}{500}\right)^{-EAE} \quad (1)$$

The interpolation of AOD data from 500 nm to 550 nm was conducted with the aim of ensuring coherence and uniformity with the AOD extinction for Black Carbon (EAOD-BC) data, which are within the 550 nm range. This approach enables a more robust analysis of the data and facilitates comparisons between different measurements, thereby enhancing our understanding of the obtained results.

2.2.2. MERRA-2

In pursuit of gaining a deeper understanding of Black Carbon (BC) concentration in the Legal Amazon region, we employed the EAOD-BC approach. Unlike AOD, EAOD-BC is a specialized index focused exclusively on BC evaluation. Numerous studies have delved into BC assessment through the absorption mode, as demonstrated in the works of Morais et al. [28]28 and Dehkhoda et al. [29]. From a different perspective, the study by Rushingabigwi et al. [30]30 analyzes the extinction mode, resembling the approach utilized in our present study.

To evaluate EAOD-BC over the Legal Amazon, we utilized the Modern-Era Retrospective Analysis for Research and Applications, version 2 (MERRA-2). It is NASA latest reanalysis system for the satellite era, starting from 1980 [31,32]. This updated system builds upon its predecessor by incorporating more observations and improvements to the Goddard Earth Observing System, version 5 (GEOS-5), produced by NASA Global Modeling and Assimilation Office (GMAO) [33]. MERRA-2 offers several enhancements over its previous version (MERRA-1), including aerosol assimilation throughout the analysis period [31–33].

The current system refinement takes into account the incorporation and analysis of satellite-derived data, as well as the application of aerosol transport models. Such improvements have a significant impact on the accuracy of BC and other aerosol estimates [32]. Satellite data from the MERRA-2 system include information from the Moderate Resolution Imaging Spectroradiometer (MODIS) sensor to estimate BC concentration in the atmosphere [31]. For the collection of the time series of EAOD-BC data in Alta Floresta, Ji-Paraná, and Rio Branco, selections were made based on the locations of physical sensors (radiometers) from AERONET between the years 2006 and 2011 (Table 1).

Preprints (www.preprints.org) | NOT PEER-REVIEWED | Posted: 1 October 2023 doi:10.20944/preprints202310.0017.v1

2.3. Specific Humidity Anomaly

In the assessment of Specific Humidity Anomaly (QA) at 2 meters above the surface, we computed the climatology using data from the MERRA-2 model (version M2TMNXSLV v5.12.4), spanning the temporal range from 1980 to 2020 (Table 1). Subsequently, monthly anomaly calculations were performed during the investigation period from 2006 to 2011. To collect the time series of QA data in Alta Floresta, Ji-Paraná, and Rio Branco, selections were made based on the locations of physical sensors (radiometers) from AERONET between the years 2006 and 2011 (Table 1).

2.4. Statistical Methodology

In the realm of statistical evaluation, we employed the Windowed Cross Correlation (WCC) technique, which assesses the lagged relationship between time series, taking into account the periodic characteristics of these time series. As described by Boker et al. [34]34, the WCC method is capable of quantifying associative variability. Within this context, WCC should track changes in the temporal lag (also known as delay) and the strength of association between both time series throughout the experiment (sampling).

With some limitations, the method aims to estimate the time interval between measurements where the maximum association occurs between the two time series and the strength of this association. The importance of finding the optimal association delay has been emphasized in previous studies, such as Zhang et al. [35]. The method should provide an estimate of the temporal delay between the event in X $\{X_1, X_2, \ldots, X_N\}$ and the event in Y $\{Y_1, Y_2, \ldots, Y_N\}$, as well as the strength of the association between the two events. In the statistical analysis, we considered the time series from the Niño 3.4 region, which effectively represents the distinct phases of ENSO. Additionally, we used the EAOD-BC and AOD 550 nm series for all three sites. To address gaps in missing AOD 550 nm data, we opted to apply linear interpolation to these series. The WCC between two time series X = Niño 3.4 and Y = Atmospheric Aerosols (AOD and EAOD-BC) with a delay β is given by Equation 2:

$$WCC(X,Y,\beta) = \frac{1}{N - \beta} \sum_{i=1}^{N-\beta} \frac{(x_i - \bar{X})(y_{i+\beta} - \bar{Y})}{std(X)\, std(Y)} \quad (2)$$

Where $\bar{X}$ and $\bar{Y}$ represent the overall means, and std(X) and std(Y) represent the standard deviations of X and Y, respectively, across all measurement instances. This method is essentially a standard Pearson correlation between the two time series lagged by observations.

3. Results

3.1. Time Series Analysis

Figure 3 illustrates the temporal variability of the ENSO indicators during the period from 2006 to 2011 in the Niño regions (Figures 3a-d) and the SOI (Figure 3e), situated in the Pacific Ocean. Within this temporal span, four ENSO events were identified, comprising two El Niños and two La Niñas. The first El Niño, depicted in red, occurred in the years 2006 and 2007, while the second one took place between 2009 and 2010. In contrast, the La Niña periods, highlighted in blue, spanned from 2007 to 2008 and from 2010 to 2011. Segments where no prominent red or blue highlights are observed represent periods of neutrality. The identification of ENSO events was based on the five time series in Figure 3, in conjunction with the widely adopted classifications found in the studies of Trenberth [34,36] and Cai et al. [22], along with the ONI index available at https://psl.noaa.gov/data/climateindices/list/.

Preprints (www.preprints.org) | NOT PEER-REVIEWED | Posted: 1 October 2023 doi:10.20944/preprints202310.0017.v1

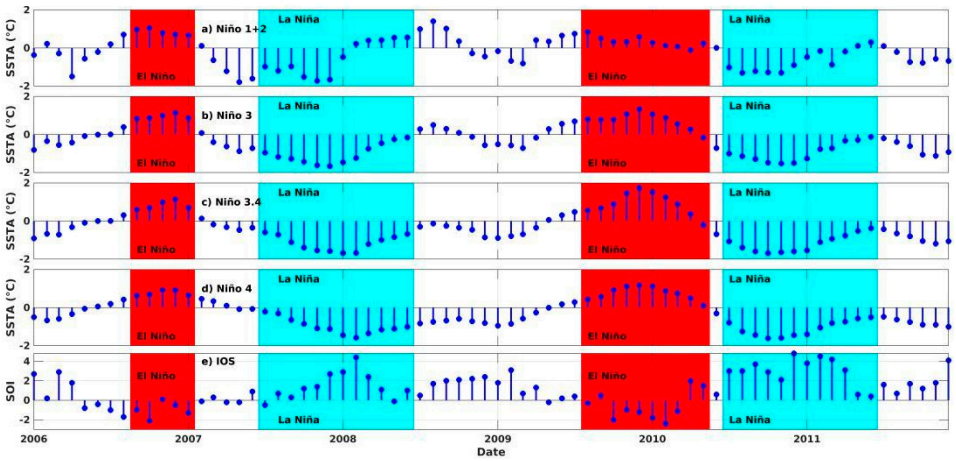

Figure 3. Time series corresponding to ENSO indicators, sea surface temperature anomalies (SSTA) over Niño regions(**a**) 1+2, (**b**) 3, (**c**) 3.4, and (**d**) 4, and (**e**) Southern Oscillation Index (SOI).

The time series of the AOD at 550 nm from the AERONET is depicted in Figure 4 for the sites in Alta Floresta, Ji Paraná, and Rio Branco. All sites exhibit a noticeable seasonality during the period spanning from 2006 to 2011, as expected due to significant emissions resulting from fires that occur during the dry season [28,37]. Sites located in the Legal Amazon region manifest distinct variability characteristics throughout the year, highlighting both a wet season and a dry season. The first half of the year is classified as the wet season, whereas the second half is characterized as the dry season, a categorization previously established by [28,38].

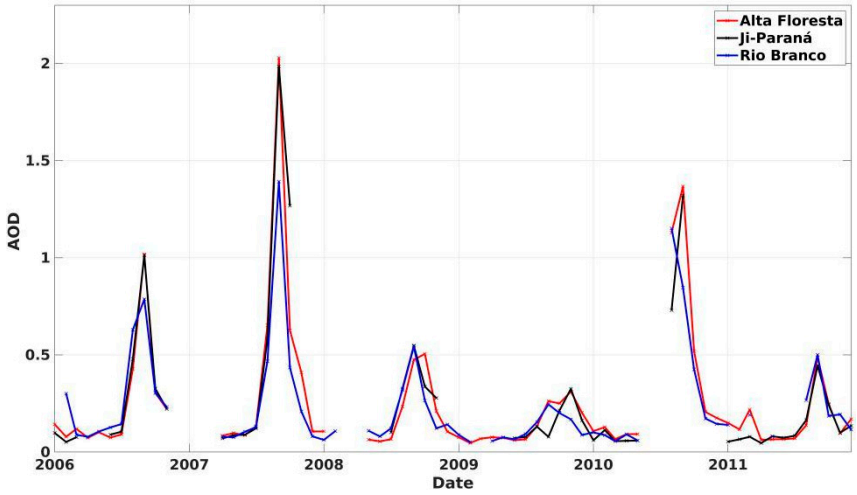

Figure 4. Time series of aerosol optical depth (AOD) at 550 nm from AERONET with monthly averages for the sites of Alta Floresta, Ji-Paraná, and Rio Branco.

During the wet season, natural and anthropogenic emissions prevail, whereas during the dry season, due to emissions from both natural and anthropogenic fires, atmospheric aerosol concentrations increase significantly, resulting in elevated AOD estimates [39]. The time series exhibit substantial data gaps during the wet season, attributed to the high cloud cover and precipitation in the Amazon region.

Similar to AOD estimates, which provide a broader view of aerosol concentrations, Figure 5 illustrates the exclusive temporal variability of EAOD-BC, derived from the MERRA-2 model, for the locations of Alta Floresta, Ji Paraná, and Rio Branco.

Preprints (www.preprints.org) | NOT PEER-REVIEWED | Posted: 1 October 2023 doi:10.20944/preprints202310.0017.v1

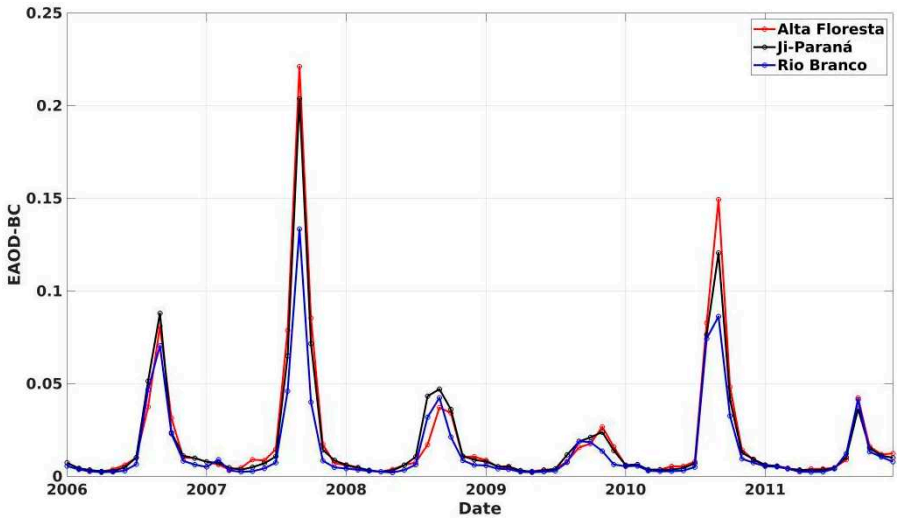

Figure 5. Time series of aerosol optical depth extinction for Black Carbon (EAOD-BC) at 550 nm with monthly averages for Alta Floresta, Ji-Paraná, and Rio Branco.

The EAOD-BC exhibits an annual variability similar to that of AOD, displaying seasonality in both the dry and wet seasons. It is worth emphasizing that EAOD-BC estimates bear a remarkable resemblance to AOD. During the wet season, EAOD-BC values hover around 0.01, while in the dry season, higher values are observed, reaching approximately 0.15 to 0.2 for Alta Floresta. Holanda et al. [8] underscore that the Amazon biome harbors a significant concentration of BC derived from emissions resulting from biomass combustion, encompassing both forest fires and burnings employed for deforestation and agricultural activities. In this context, these anthropogenic actions release substantial quantities of particulate matter into the atmosphere, with BC being one of the predominant elements among atmospheric aerosols in the region under study.

According to [28], in the deforestation arc region BC contribution is dominant during the dry season. To some extent, all locations in the deforestation arc exhibit aerosol concentrations with a mixture of dust, BC, and Brown Carbon (BrC). These values possibly result from the long-distance (intercontinental) transport of Saharan and regional aerosol plumes, which initially arrive in the Alta Floresta region and subsequently move towards Ji-Paraná and Rio Branco regions [8].

3.2. Windowed Cross-Correlation

Utilizing the WCC (Figures 6 and 7) allows for a more nuanced understanding of the dynamic interactions between the time series, enabling the identification of lags and contributing to a precise data analysis and interpretation. Figures 6 and 7 illustrate the temporal relationship between the ENSO indicator, the SSTA in the Niño 3.4 region, and the AOD estimates (Figure 6) and EAOD-BC (Figure 7) during the period from 2006 to 2011. We will examine negative lags, which represent the delay of AOD and EAOD-BC estimates concerning the ENSO indicator time series.

Preprints (www.preprints.org) | NOT PEER-REVIEWED | Posted: 1 October 2023 doi:10.20944/preprints202310.0017.v1

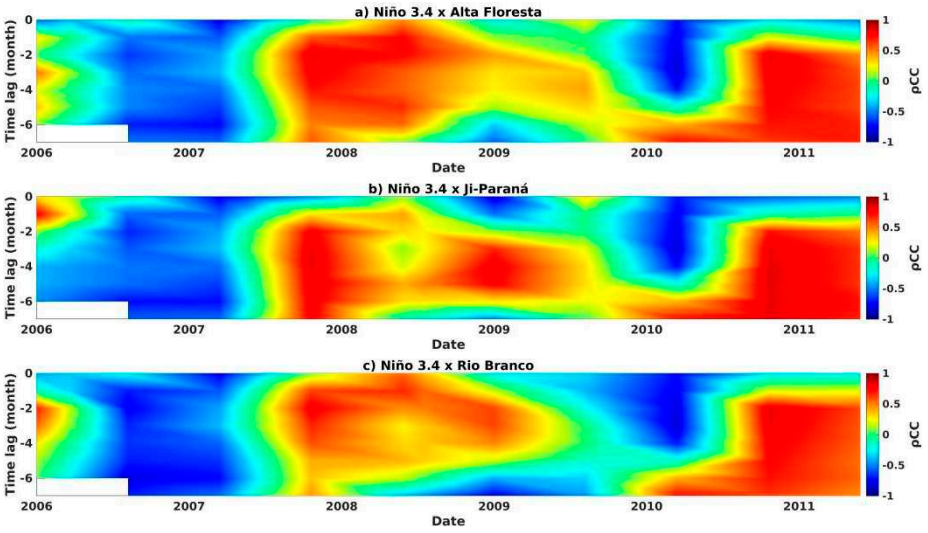

Figure 6. Windowed cross-correlation (WCC) analysis between the time series of SST anomalies (SSTA) in the Niño 3.4 region and the time series of aerosol optical depth (AOD) at 550 nm for (**a**) Alta Floresta, (**b**) Ji-Paraná, and (**c**) Rio Branco.

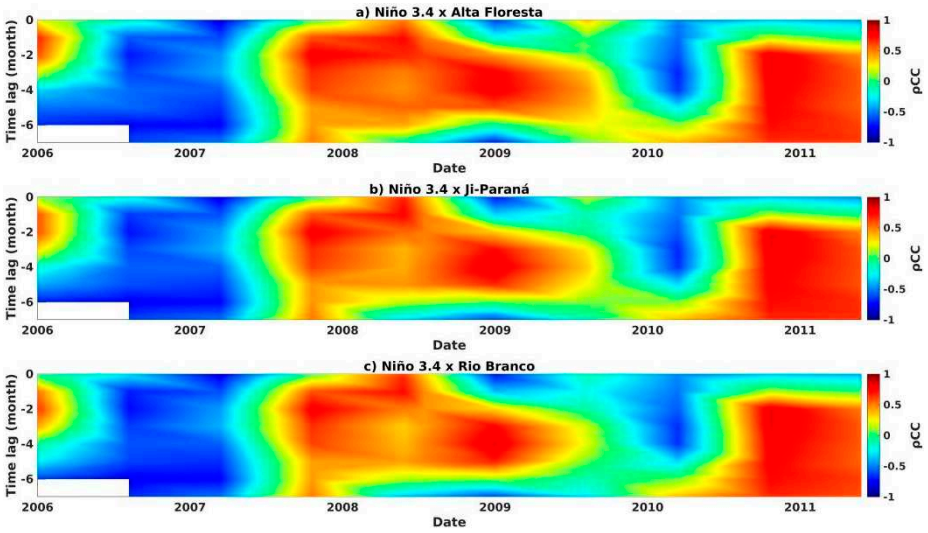

Figure 7. Windowed cross-correlation (WCC) analysis between the time series of SSTA (SSTA) in the Niño 3.4 region and the time series of aerosol optical depth extinction for Black Carbon (EAOD-BC) at 550 nm for the sites of (**a**) Alta Floresta, (**b**) Ji-Paraná, and (**c**) Rio Branco.

In general, all the conducted analyses have revealed a consistent relationship between the ENSO indicator and atmospheric aerosols, displaying a consistent pattern of lag and cross-correlation coefficients (ϱCC) throughout the entire analysis period at the three sites. Observing Figures 6 and 7 during the analysis period, ϱCC oscillated between positive and negative values. Between 2007 and 2008, negative ϱCC values (approximately -0.7) were identified with lags of up to 6 months, indicating that the time series were out of phase during this period. Increases (or decreases) in the ENSO indicator led to decreases (or increases) in AOD and EAOD-BC estimates.

Conversely, between 2007 and 2009, positive ϱCC values were observed, also with a lag of up to 6 months, suggesting that the time series were in phase during this period. Increases (or decreases) in the ENSO indicator resulted in increases (or decreases) in AOD and EAOD-BC estimates. It is noteworthy that during this period, for AOD in Ji-Paraná (Figure 6b) and Rio Branco (Figure 6c), some fluctuations in ϱCC were observed, along with lower ϱCC values, around 0 to 0.5, indicating a lack of statistical significance.

Preprints (www.preprints.org) | NOT PEER-REVIEWED | Posted: 1 October 2023 doi:10.20944/preprints202310.0017.v1

Towards the end of 2009 until 2011, both negative and positive ϱCC were found for all analyses, with positive ϱCC predominantly during this period. Between 2009 and 2010, a lag of up to 4 months was observed between the ENSO indicator and atmospheric aerosols, with ϱCC approximately -0.8 for AOD and approximately -0.6 for EAOD-BC (Figure 7), both statistically significant. During this period, increases (or decreases) in the ENSO indicator resulted in decreases (or increases) in AOD and EAOD-BC. Hence, atmospheric aerosols were out of phase with the ENSO indicator.

In the period from 2010 to 2011, ϱCC predominantly displayed positive values, exceeding 0.65. These values were observed for the locations of Alta Floresta (Figure 6a) and Ji-Paraná (Figure 6b), reaching approximately 0.75, with higher statistical significance. Until the middle of 2010, regarding EAOD-BC (Figure 7), there was not as much statistical significance in the ϱCC value compared to the AOD analysis until the middle of 2010. However, concerning AOD, a lag ranging from 5 to over 6 months in relation to the ENSO indicator was observed until the middle of 2010. From the middle of 2010 until the end of the series, higher ϱCC values were observed, which stood out as the maximum values throughout the entire analysis, with lags of up to 6 months. Consequently, it was found that increases (or decreases) in the ENSO indicator resulted in increases (or decreases) in atmospheric aerosols, indicating that the time series were in phase with a lag of up to 6 months.

3.3. Spatio Temporal Assessment

Through a meticulous examination of the time series of ENSO indicators (Figure 3), along with AOD estimates (Figure 4) and EAOD-BC (Figure 5), and further delving into this assessment using WCC (Figures 6 and 7), it is possible to identify two similar scenarios during the El Niño and La Niña periods. In both cases, El Niño periods were evident: the first occurred between September 2006 and January 2007 (EN-0607), lasting for five months (Figure 8a); the second spanned from August 2009 to May 2010 (EN-0910), encompassing a duration of ten months (Figure 9a).

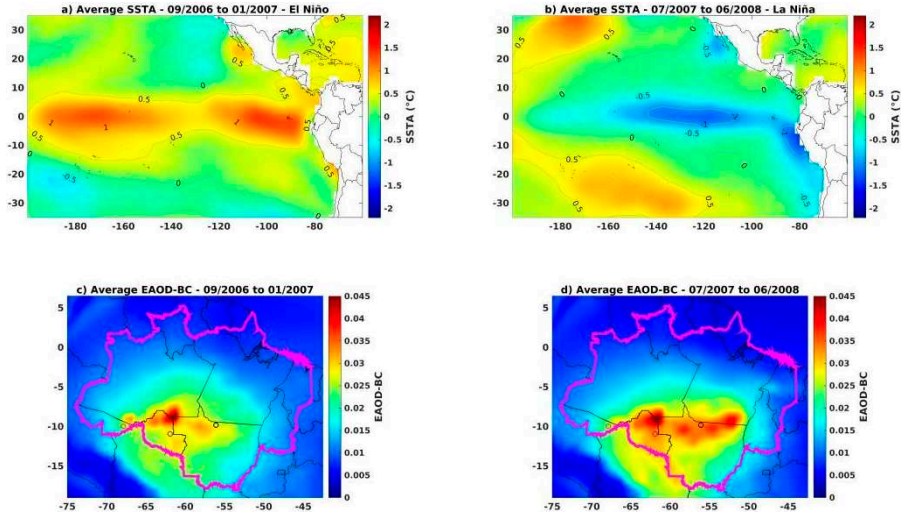

Figure 8. Evaluation over the Pacific Ocean showing a) average SSTA during the period 09/2006 to 01/2007, covering the El Niño period, b) average SSTA during the period 07/2007 to 06/2008, covering the La Niña period, and average spatial distribution of extinction aerosol optical depth extinction for Black Carbon (EAOD-BC) at 550 nm during the periods c) El Niño and d) La Niña.

Preprints (www.preprints.org) | NOT PEER-REVIEWED | Posted: 1 October 2023 doi:10.20944/preprints202310.0017.v1

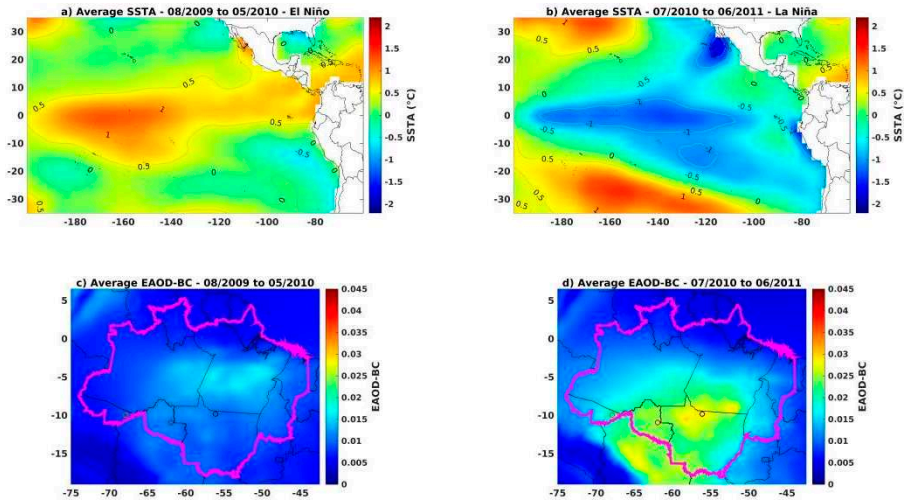

Figure 9. Evaluation over the Pacific Ocean showing a) average SSTA during the period 08/2009 to 05/2010, covering the El Niño period, b) average SSTA during the period 07/2010 to 06/2011, covering the La Niña period, and average spatial distribution of aerosol optical depth extinction for Black Carbon (EAOAD-BC) at 550 nm during the periods c) El Niño and d) La Niña.

Following these two El Niño periods, La Niña years were identified, each lasting for 12 months: one between July 2007 and June 2008 (LN-0708), and another between July 2010 and June 2011 (LN-1011). During these La Niña periods, there was a significant increase in AOD, as observed in the time series (Figure 4), as well as an increase in EAOD-BC, as evidenced in the time series (Figure 5), with detailed spatial analyses of the Legal Amazon region illustrated in Figures 8c-d and 9c-d.

In the analysis conducted through WCC, statistical significance was found between the ENSO indicator and atmospheric aerosols. The ϱCC reached its minimum values between the years 2006 and 2007, with a delay of approximately 6 months. After the increase in AOD and EAOD-BC estimates throughout the year 2006, reductions in SST were observed in all Niño regions, with a lag of approximately six months. The ENSO phase exhibited an opposite phase to that of atmospheric aerosols during the six-month period between 2006 and 2007, supporting the perspective of an increase in atmospheric aerosols in LN-0708 as a result of the EN-0607 event. This relationship becomes evident when analyzing EAOD-BC estimates in the Legal Amazon region, where significant increases in EAOD-BC were observed, especially at the locations of the three AERONET network sites, as demonstrated in Figures 8c and 8d.

Examining oceanic characteristics during the EN-0607 (Figure 8a) and LN-0708 (Figure 8b) periods, in conjunction with variations in EAOD-BC estimates over the Legal Amazon region between these two events, a considerable increase in EAOD-BC estimates over the central-southern region of the Legal Amazon was observed. The border region comprising the states of Rondônia, Amazonas, and Mato Grosso remained stable in terms of estimates. However, on a broader scale, in the central-southern portion of the biome, a significant increase was noted after the EN-0607 period, during the LN-0708 coverage. The time series (Figures 4 and 5) revealed increases of approximately 100% in the peaks of AOD and EAOD-BC between the intervals of these events. In the northwest, north, and northeast regions of the biome, conditions remained consistent, with low EAOD-BC estimates and no significant changes.

As highlighted by Cai et al. [22], the year 2007 was categorized as a CP/Modoki La Niña event. The authors suggest that the onset of this specific La Niña phenomenon (during the months of June, July, and August) implies positive anomalies in air temperatures in the area covered by the deforestation arc, precisely where significant increases in EAOD-BC were observed. This atmospheric condition can be identified as a determining factor for the increase in atmospheric aerosol estimates, particularly EAOD-BC, as forest fires become more recurrent and susceptible during this period due to abnormal air temperature variations. Consequently, there is an intensification in aerosol and pollutant emissions into the atmosphere.

Preprints (www.preprints.org) | NOT PEER-REVIEWED | Posted: 1 October 2023 doi:10.20944/preprints202310.0017.v1

Between the years 2009 and 2011, a similar situation to the previous one was observed, as illustrated in Figure 8. This scenario was characterized by an increase in EAOD-BC estimates after an El Niño period, followed by a La Niña event. It is crucial to highlight the disparities in the prevailing oceanic conditions between these periods. Comparing Figures 8 and 9, both the EN-0607 event (Figure 8a) and the LN-1011 event (Figure 9b) manifested more strongly, as evidenced by SSTA in the Pacific Ocean, unlike the EN-0910 (Figure 8a) and LN-0708 (Figure 7b) events, which occurred weaker in terms of SSTA . For EAOD-BC estimates, lower values were obtained in these latter two ENSO events (Figures 9c and 9d), as well as in the time series of AOD and EAOD-BC for the three sites.

It is worth noting that during the ENOS episodes that occurred between 2006 and 2008, SST anomalies exhibited different distributions between the central and coastal regions of the Pacific Ocean. In contrast to these ENOS events, which occurred between 2009 and 2011, a concentration of higher SSTA was observed for EN-0910 and lower SSTA for LN-1011 in the central portion of the Pacific Ocean. This analysis assumes primary relevance due to the ocean-atmosphere interaction, which presumably exerted influence on atmospheric aerosol estimates over the Legal Amazon region.

In the period from 2009 to 2011, ϱCC values were found to oscillate between positive and negative, with a maximum lag of approximately 4 to 6 months between the ENSO indicator and atmospheric aerosols. Similar to the analysis represented in Figure 8, there was an increase of over 100% in AOD and EAOD-BC peaks during the interval corresponding to the occurrence of El Niño and La Niña phenomena (ENSO).

Regarding EAOD-BC in the Legal Amazon region, during the EN-0910 event (Figure 8a), the most significant estimates were observed in the areas east of the Amazon and in the central part of Pará. Subsequently to this event, during the LN-1011 period (Figure 9b), changes in the distribution of EAOD-BC (Figure 9c and 9d) occurred across virtually the entire extent of the Legal Amazon. It is worth noting in this context that the central-southern portion of the biome presented the most significant estimates, with Alta Floresta and Ji-Paraná particularly more affected compared to Rio Branco. Similar to Figure 8, in Figure 9, in the deforestation arc area where the three sites are located, they are evidently the most impacted by EAOD-BC.

In all four periods analyzed, the state of Rondônia consistently exhibits EAOD-BC values above 0.025 across virtually its entire area, reaching approximately 0.045 in some periods. These values are considerably higher compared to other states. The state of Mato Grosso presents a situation similar to that of Roraima, with the northern part of the state being significantly affected. In time series analyses, this trend becomes more evident, especially through AOD, which provides a more precise representation of atmospheric aerosol concentrations. The southern regions of the Amazonas and Pará states were the most impacted due to their location, as they are part of the deforestation arc. On the other hand, the states of Roraima, Tocantins, and Maranhão showed less pronounced influence of EAOD-BC in the four periods analyzed.

It is essential to conduct a detailed analysis of the two scenarios presented, in which the decrease in SST resulted in La Niña events. As a result, there was an increase in AOD and EAOD-BC estimates, which is an unusual situation since in La Niña years, meteorological and environmental conditions typically favor a decrease in atmospheric aerosol estimates in the Legal Amazon region, where the study is situated.

4. Discussion

According to Nascimento; Senna [40], the scenario illustrated in Figure 9 can be attributed to the La Niña event being classified as CP/Modoki. This classification entails an atmospheric teleconnection mechanism that influences meteorological variables, resulting in an increased risk of wildfires. As for the case depicted in Figure 8, the assessment conducted by Palácios et al. [37] revealed that the year 2007 exhibited the highest number of wildfire incidents between 2002 and 2017. During this period, variations in atmospheric aerosols directly correlate with the surge in wildfire occurrences, with wildfires serving as a major source of aerosol emissions within the study area. In accordance with the findings of Barbosa et al. [41], there was a notable uptick in the incidence of wildfires and

Preprints (www.preprints.org) | NOT PEER-REVIEWED | Posted: 1 October 2023 doi:10.20944/preprints202310.0017.v1

affected areas during La Niña events. The authors indicate that meteorological factors, in conjunction with social and environmental aspects, play a pivotal role in influencing these variables.

In this context, comprehending these two scenarios can be grounded in the study by Silva Junior et al. [42], which emphasizes that stronger trade winds have the potential to propagate wildfires, a phenomenon exacerbated during La Niña periods. The circulation of trade winds originating from the northeast exhibits greater velocity, thereby accelerating the dynamics of wildfires in the region. It is crucial to highlight that trade winds exert a significant impact on the occurrence and spread of wildfires, provided favorable conditions of temperature and relative humidity exist. These winds, renowned for their regularity and constancy, can expedite the combustion of biomass and facilitate the rapid spread of fires across extensive areas. In summary, trade winds play a fundamental role in transporting particles and act as facilitators for the expansion of fires into adjacent regions.

4.1. Specific Humidity Assessment

In order to delve deeper into the preceding analyses, aiming to comprehend the periods of ENSO influence and its potential concurrent effects with meteorological characteristics in the Legal Amazon region, Figure 10 depicts the variability of specific humidity (Q) and the QA over the temporal span from 2006 to 2011 for three distinct locations: Alta Floresta (Figure 10a), Ji Paraná (Figure 10b), and Rio Branco (Figure 10c).

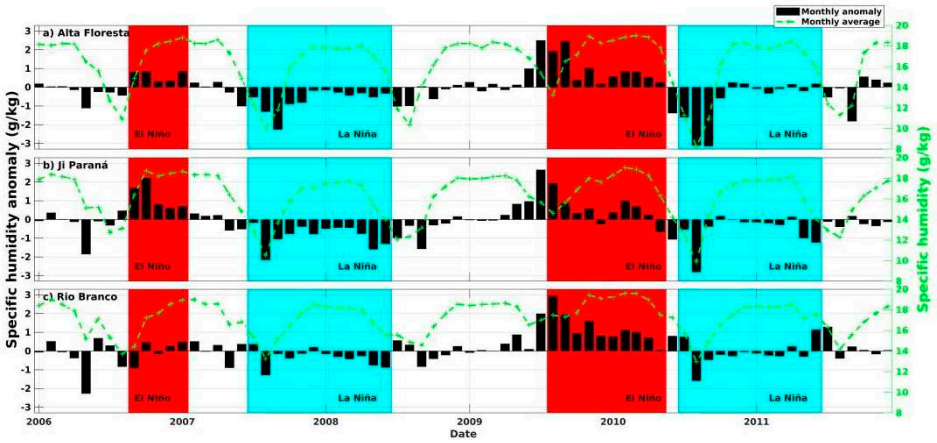

Figure 10. Time series of MERRA-2 model data between 2006 and 2011 for specific humidity (g/kg) on the dashed green lines and specific humidity anomaly (g/kg) on the black bars, based on the climatology between 1980 and 2020, both series based on the locations of AERONET sites for a) Alta Floresta, b) Ji Paraná, and c) Rio Branco. The red and blue highlights indicate the periods of El Niño and La Niña, respectively.

During the EN-0607 and EN-0910 episodes, positive values of QA prevail across all sites, with Q levels exceeding 14 g/kg. It is worth noting that during these El Niño periods, higher SH rates are observed over the biome. Importantly, these El Niño events coincide with the phase categorized as the dry season of atmospheric aerosols. In these two events, the lowest estimates of AOD and EAOD-BC were observed compared to subsequent La Niña events. Conversely, during the LN-0708 and LN-1011 episodes, QA predominantly exhibited negative values, especially at the onset of each event. Remarkably, for Rio Branco (Figure 10c), elevated Q and QA were observed, conditions conducive to obtaining the lowest estimates of AOD and EAOD-BC.

The El Niño and La Niña scenarios discussed here stand out for their notable uniqueness when contrasted with widely discussed studies and average patterns characterizing events affecting the Amazon region. According to Foley et al. [43], in the Amazon region, El Niño episodes are associated with warmer and drier meteorological conditions than the usual pattern. Conversely, La Niña events bring cooler and moister environmental conditions. Focusing on the hydrological aspect, variations resulting from ENSO influence both soil and air humidity in the Amazon, mediated by alterations in rainfall rates. However, Withey et al. [44] emphasize the need to incorporate forest fire occurrences

associated with El Niño when estimating carbon emissions from the Amazon region. In this perspective, substantial differences were identified in this study, resulting in increases in atmospheric aerosol estimates during La Niña episodes and the opposite trend for El Niño events. Thus, by examining changes over time in Q and QA, in conjunction with ENSO climate patterns, it becomes possible to recognize complex and significant connections between climatic events and atmospheric conditions in the Legal Amazon.

According to Sousa et al. [45], it is plausible to infer that El Niño exerts a substantial influence on subsequent precipitation rates in specific areas of the Amazon region. This observation aligns with the analysis by Souza et al. [46], who, through statistical analysis, demonstrate a statistically significant relationship between atmospheric aerosols and precipitation.

In this context, the temporal discrepancies detected, as evidenced through the WCC, between ENSO events and the distribution of AOD and EAOD-BC in the Legal Amazon, could possibly be attributed to changes in rainfall patterns in the studied region. However, such temporal gaps may also be associated with the QA identified within the scope of the region under examination.

5. Conclusions

This study presents the results of the assessment of the relationship between ENSO and estimates of atmospheric aerosol concentrations, using the metrics of AOD and EAOD-BC, over the Legal Amazon region, including the AERONET sites located within the biome, namely Alta Floresta, Ji Paraná, and Rio Branco, between 2006 and 2011. After applying statistical evaluations using WCC between ENSO indicators and atmospheric aerosol estimates, as well as analyzing ENSO events in conjunction with spatial assessment of EAOD-BC, the most relevant conclusions are as follows:

Through the WCC analyses conducted across all investigated contexts, a consistent relationship between the ENSO indicator and atmospheric aerosol estimates was evidenced, manifested by a lag pattern and cross-correlation coefficients (ϱCC) that remained consistent throughout the analyzed period at the three study locations. Statistically significant lags of up to 4 to 6 months were observed between the ENSO indicator and atmospheric aerosol estimates, indicating the existence of delays in AOD and EAOD-BC estimates.

Following a comprehensive analysis of time series data, combining lag statistical assessments and spatiotemporal analysis, two similar scenarios were identified during the El Niño and La Niña periods. During these La Niña periods, a significant increase in AOD values was observed in the time series, as well as an increase in EAOD-BC values. This finding supports the perspective of an increase in atmospheric aerosol levels during La Niña events, especially in the category of La Niña CP (Central Pacific)/Modoki. Such an increase can be understood as a response to previous El Niño events. It is noteworthy that after these El Niño episodes, in the subsequent La Niña period, particularly during the dry season, an increase of over 100% in AOD and EAOD-BC estimates was identified compared to the El Niño influence period. The characteristics observed in this study, occurring between 2006 and 2011, are considered atypical. This is justified by the fact that, during La Niña years, meteorological and environmental conditions typically lead to a reduction in atmospheric aerosol estimates in the Legal Amazon region, where this study is situated. In this context, it is highlighted that the central-southern portion of the Legal Amazon presented the most significant EAOD-BC estimates, with Alta Floresta and Ji-Paraná sites being particularly more affected compared to Rio Branco.

When analyzing the QA, exceptional situations were identified in comparison to previous investigations and the characteristic average patterns of events affecting the Amazon region. During El Niño events, nearly 100% positive QA values were observed. In contrast, during La Niña years, pronounced negative values were identified in the early months of the event's influence.

Author Contributions: Conceptualization, A.G.C.P., R.P., P.C.R.S, and R.V.S.P.; methodology, A.G.C.P., R.P., G.C., and B.I.; data curation, data processing and analysis, A.G.C.P., R.P., P.C.R.S, and R.V.S.P.; interpreted the analysis results, A.G.C.P., R.P., P.C.R.S, R.V.S.P., G.C., and B.I.; formal analysis, A.G.C.P., R.P., R.V.S.P., and G.C.; writing—original draft preparation, A.G.C.P.; writing—review and editing, A.G.C.P., R.P., P.C.R.S., R.V.S.P., G.C., and B.I.; visualization, A.G.C.P., R.P., P.C.R.S., R.V.S.P., G.C., B.I.; supervision, R.P., G.C., and B.I.; project administration, A.G.C.P., R.P., G.C.; funding acquisition, R.P. All authors have read and agreed to the published version of the manuscript.

Funding: This work was supported by UFPA ("Universidade Federal do Pará"; Federal University of Pará) under the projects PRO4463-2020, PRO3906-2019, and the PAPQ ("Programa de Apoio à Publicação Qualificada"; Qualified Publication Support Program).

Data Availability Statement: Data Availability Statement: All the data used in this study are publicly available for free. Therefore, please refer to Section 2 for the sources in the materials and

Acknowledgments: The authors express their gratitude for the financial support provided by the PAPQ ("Programa de Apoio à Publicação Qualificada"; Qualified Publication Support Program) affiliated with UFPA ("Universidade Federal do Pará"; Federal University of Pará).

Conflicts of Interest: The authors declare no conflict of interest.

References

1. Schöngart, J.; Junk, W. J.; Piedade, M. T. F.; Ayres, J. M.; Hüttermann, A.; Worbes, M. Teleconnection between Tree Growth in the Amazonian Floodplains and the El Niño-Southern Oscillation Effect: DENDROCLIMATIC RECORD OF AMAZON FLOODPLAINS. *Glob. Change Biol.* **2004**, *10*, 683–692. https://doi.org/10.1111/j.1529-8817.2003.00754.x.
2. Aragão, L. E. O. C.; Poulter, B.; Barlow, J. B.; Anderson, L. O.; Malhi, Y.; Saatchi, S.; Phillips, O. L.; Gloor, E. Environmental Change and the Carbon Balance of Amazonian Forests: Environmental Change in Amazonia. *Biol. Rev.* **2014**, *89*, 913–931. https://doi.org/10.1111/brv.12088.
3. Li, F.; Lin, W.; Jiang, B.; Li, J. Investigation of Aerosol Direct Effect over China under El Niño and Its Spatial Distribution Using WRF-Chem. *Atmosphere* **2020**, *12*, 58. https://doi.org/10.3390/atmos12010058.
4. Zhou, Y.; Yan, H.; Luo, J.-J. Impacts of Amazon Fire Aerosols on the Subseasonal Circulations of the Mid-High Latitudes. *Front. Earth Sci.* **2021**, *8*, 609554. https://doi.org/10.3389/feart.2020.609554.
5. Huijnen, V.; Wooster, M. J.; Kaiser, J. W.; Gaveau, D. L. A.; Flemming, J.; Parrington, M.; Inness, A.; Murdiyarso, D.; Main, B.; Van Weele, M. Fire Carbon Emissions over Maritime Southeast Asia in 2015 Largest since 1997. *Sci. Rep.* **2016**, *6*, 26886. https://doi.org/10.1038/srep26886.
6. Artaxo, P.; Hansson, H.-C.; Andreae, M. O.; Bäck, J.; Alves, E. G.; Barbosa, H. M. J.; Bender, F.; Bourtsoukidis, E.; Carbone, S.; Chi, J.; et al. Tropical and Boreal Forest – Atmosphere Interactions: A Review. *Tellus B Chem. Phys. Meteorol.* **2022**, *74*, 24-163. https://doi.org/10.16993/tellusb.34.
7. Alves, N. O.; Brito, J.; Caumo, S.; Arana, A.; De Souza Hacon, S.; Artaxo, P.; Hillamo, R.; Teinilä, K.; Batistuzzo De Medeiros, S. R.; De Castro Vasconcellos, P. Biomass Burning in the Amazon Region: Aerosol Source Apportionment and Associated Health Risk Assessment. *Atmos. Environ.* **2015**, *120*, 277–285. https://doi.org/10.1016/j.atmosenv.2015.08.059.
8. Holanda, B. A.; Pöhlker, M. L.; Walter, D.; Saturno, J.; Sörgel, M.; Ditas, J.; Ditas, F.; Schulz, C.; Franco, M. A.; Wang, Q.; et al. Influx of African Biomass Burning Aerosol during the Amazonian Dry Season through Layered Transatlantic Transport of Black Carbon-Rich Smoke. *Atmospheric Chem. Phys.* **2020**, *20*, 4757–4785. https://doi.org/10.5194/acp-20-4757-2020.
9. Holanda, B. A.; Franco, M. A.; Walter, D.; Artaxo, P.; Carbone, S.; Cheng, Y.; Chowdhury, S.; Ditas, F.; Gysel-Beer, M.; Klimach, T.; et al. African Biomass Burning Affects Aerosol Cycling over the Amazon. *Commun. Earth Environ.* **2023**, *4*, 154. https://doi.org/10.1038/s43247-023-00795-5.
10. Bond, T. C.; Bergstrom, R. W. Light Absorption by Carbonaceous Particles: An Investigative Review. *Aerosol Sci. Technol.* **2006**, *40*, 27–67. https://doi.org/10.1080/02786820500421521.
11. Bond, T. C.; Doherty, S. J.; Fahey, D. W.; Forster, P. M.; Berntsen, T.; DeAngelo, B. J.; Flanner, M. G.; Ghan, S.; Kärcher, B.; Koch, D.; et al. Bounding the Role of Black Carbon in the Climate System: A Scientific Assessment: BLACK CARBON IN THE CLIMATE SYSTEM. *J. Geophys. Res. Atmospheres* **2013**, *118*, 5380–5552. https://doi.org/10.1002/jgrd.50171.
12. Forbes, M. S.; Raison, R. J.; Skjemstad, J. O. Formation, Transformation and Transport of Black Carbon (Charcoal) in Terrestrial and Aquatic Ecosystems. *Sci. Total Environ.* **2006**, *370*, 190–206. https://doi.org/10.1016/j.scitotenv.2006.06.007.
13. Barkley, A. E.; Prospero, J. M.; Mahowald, N.; Hamilton, D. S.; Popendorf, K. J.; Oehlert, A. M.; Pourmand, A.; Gatineau, A.; Panechou-Pulcherie, K.; Blackwelder, P.; et al. African Biomass Burning Is a Substantial Source of Phosphorus Deposition to the Amazon, Tropical Atlantic Ocean, and Southern Ocean. *Proc. Natl. Acad. Sci.* **2019**, *116*, 16216–16221. https://doi.org/10.1073/pnas.1906091116.
14. Lou, S.; Yang, Y.; Wang, H.; Lu, J.; Smith, S. J.; Liu, F.; Rasch, P. J. Black Carbon Increases Frequency of Extreme ENSO Events. *J. Clim.* **2019**, *32*, 8323–8333. https://doi.org/10.1175/JCLI-D-19-0549.1.
15. Kim, M.-K.; Lau, W. K. M.; Kim, K.-M.; Sang, J.; Kim, Y.-H.; Lee, W.-S. Amplification of ENSO Effects on Indian Summer Monsoon by Absorbing Aerosols. *Clim. Dyn.* **2016**, *46*, 2657–2671. https://doi.org/10.1007/s00382-015-2722-y.

16. Feng, J.; Zhu, J.; Li, J.; Liao, H. Aerosol Concentrations Variability over China: Two Distinct Leading Modes. *Atmospheric Chem. Phys.* **2020**, *20*, 9883–9893. https://doi.org/10.5194/acp-20-9883-2020.
17. Wang, J.; Liu, Y.; Ding, Y. On the Connection between Interannual Variations of Winter Haze Frequency over Beijing and Different ENSO Flavors. *Sci. Total Environ.* **2020**, *740*, 140109. https://doi.org/10.1016/j.scitotenv.2020.140109.
18. Oliveira, F. P.; Oyama, M. D. Squall-line Initiation over the Northern Coast of Brazil in March: Observational Features. *Meteorol. Appl.* **2020**, *27*, e1799. https://doi.org/10.1002/met.1799.
19. Rizzo, L. V.; Artaxo, P.; Müller, T.; Wiedensohler, A.; Paixão, M.; Cirino, G. G.; Arana, A.; Swietlicki, E.; Roldin, P.; Fors, E. O.; et al. Long Term Measurements of Aerosol Optical Properties at a Primary Forest Site in Amazonia. *Atmospheric Chem. Phys.* **2013**, *13*, 2391–2413. https://doi.org/10.5194/acp-13-2391-2013.
20. Pöhlker, M. L.; Pöhlker, C.; Ditas, F.; Klimach, T.; Angelis, I. H.; Araújo, A.; Brito, J.; Carbone, S.; Cheng, Y.; Chi, X.; et al. Long-Term Observations of Cloud Condensation Nuclei in the Amazon Rain Forest – Part 1: Aerosol Size Distribution, Hygroscopicity, and New Model Parametrizations for CCN Prediction. *Atmospheric Chem. Phys.* **2016**, *16*, 15709–15740. https://doi.org/10.5194/acp-16-15709-2016.
21. Saturno, J.; Holanda, B. A.; Pöhlker, C.; Ditas, F.; Wang, Q.; Moran-Zuloaga, D.; Brito, J.; Carbone, S.; Cheng, Y.; Chi, X.; et al. Black and Brown Carbon over Central Amazonia: Long-Term Aerosol Measurements at the ATTO Site. *Atmospheric Chem. Phys.* **2018**, *18*, 12817–12843. https://doi.org/10.5194/acp-18-12817-2018.
22. Cai, W.; McPhaden, M. J.; Grimm, A. M.; Rodrigues, R. R.; Taschetto, A. S.; Garreaud, R. D.; Dewitte, B.; Poveda, G.; Ham, Y. G.; Santoso, A.; et al. Climate Impacts of the El Niño–Southern Oscillation on South America. *Nat. Rev. Earth Environ.* **2020**, *1*, 215–231. https://doi.org/10.1038/s43017-020-0040-3.
23. Reboita, M. S.; Oliveira, K. R.; Corrêa, P. Y. C.; Rodrigues, R. Influence of the Different Types of El Niño in the Precipitation over South America. *Rev. Bras. Geogr. Física* **2021**, *14*, 729–742. https://doi.org/10.26848/rbgf.v14.2.p729-742.
24. Trenberth, K. E. El Niño Southern Oscillation (ENSO). *Elsevier*, **2019**, *6*, 420–432. https://doi.org/10.1016/B978-0-12-409548-9.04082-3.
25. Holben, B. N.; Eck, T. F.; Slutsker, I.; Tanré, D.; Buis, J. P.; Setzer, A.; Vermote, E.; Reagan, J. A.; Kaufman, Y. J.; Nakajima, T.; et al. AERONET—A Federated Instrument Network and Data Archive for Aerosol Characterization. *Remote Sens. Environ.* **1998**, *66*, 1–16. https://doi.org/10.1016/S0034-4257(98)00031-5.
26. Dayou, J.; Chang, J. H. W.; Sentian, J. In *Ground-Based Aerosol Optical Depth Measurement Using Sunphotometers; SpringerBriefs in Applied Sciences and Technology*, 1st ed; Springer: Kota Kinabalu, Malaysia, 2014; Volume 1, pp 1-67. https://doi.org/10.1007/978-981-287-101-5.
27. Li, J.; Ge, X.; He, Q.; Abbas, A. Aerosol Optical Depth (AOD): Spatial and Temporal Variations and Association with Meteorological Covariates in Taklimakan Desert, China. *PeerJ* **2021**, *9*, e10542. https://doi.org/10.7717/peerj.10542.
28. Morais, F. G.; Franco, M. A.; Palácios, R.; Machado, L. A. T.; Rizzo, L. V.; Barbosa, H. M. J.; Jorge, F.; Schafer, J. S.; Holben, B. N.; Landulfo, E.; et al. Relationship between Land Use and Spatial Variability of Atmospheric Brown Carbon and Black Carbon Aerosols in Amazonia. *Atmosphere* **2022**, *13*, 1328. https://doi.org/10.3390/atmos13081328.
29. Dehkhoda, N.; Sim, J.; Joo, S.; Shin, S.; Noh, Y. Retrieval of Black Carbon Absorption Aerosol Optical Depth from AERONET Observations over the World during 2000–2018. *Remote Sens.* **2022**, *14*, 1510. https://doi.org/10.3390/rs14061510.
30. Rushingabigwi, G.; Zhang, J.; Bachagha, T.; Kalisa, W.; Henchiri, M.; Shahzad, A.; Nsengiyumva, P.; Bugingo, C. N. The Influence of Dust and Black Carbon on Clouds, in Africa. *J. Comput. Commun.* **2018**, *6*, 342–352. https://doi.org/10.4236/jcc.2018.611031.
31. Buchard, V.; Randles, C. A.; Da Silva, A. M.; Darmenov, A.; Colarco, P. R.; Govindaraju, R.; Ferrare, R.; Hair, J.; Beyersdorf, A. J.; Ziemba, L. D.; Yu, H. The MERRA-2 Aerosol Reanalysis, 1980 Onward. Part II: Evaluation and Case Studies. *J. Clim.* **2017**, *30*, 6851–6872. https://doi.org/10.1175/JCLI-D-16-0613.1.
32. Randles, C. A.; Silva, A. M.; Buchard, V.; Colarco, P. R.; Darmenov, A.; Govindaraju, R.; Smirnov, A.; Holben, B.; Ferrare, R.; Hair, J.; et al. The MERRA-2 Aerosol Reanalysis, 1980 Onward. Part I: System Description and Data Assimilation Evaluation. *J. Clim.* **2017**, *30*, 6823–6850. https://doi.org/10.1175/JCLI-D-16-0609.1.
33. Gelaro, R.; McCarty, W.; Suárez, M. J.; Todling, R.; Molod, A.; Takacs, L.; Randles, C. A.; Darmenov, A.; Bosilovich, M. G.; Reichle, R.; et al. The Modern-Era Retrospective Analysis for Research and Applications, Version 2 (MERRA-2). J. Clim. 2017, 30, 5419–5454. https://doi.org/10.1175/JCLI-D-16-0758.1.
34. Boker, S. M.; Rotondo, J. L.; Xu, M.; King, K. Windowed Cross-Correlation and Peak Picking for the Analysis of Variability in the Association between Behavioral Time Series. *Psychol. Methods* **2002**, *7*, 338–355. https://doi.org/10.1037/1082-989X.7.3.338.
35. Zhang, W.; Li, Y.; Wu, X.; Chen, Y.; Chen, A.; Schwalm, C. R.; Kimball, J. S. Divergent Response of Vegetation Growth to Soil Water Availability in Dry and Wet Periods Over Central Asia. *J. Geophys. Res. Biogeosciences* **2021**, *126*, e2020JG005912. https://doi.org/10.1029/2020JG005912.

36. Trenberth, K. E. The Definition of El Niño. *Bull. Am. Meteorol. Soc.* **1997**, *78*, 2771–2777. https://doi.org/10.1175/1520-0477(1997)078<2771:TDOENO>2.0.CO;2.
37. Palácios, R.; Nassarden, D. C. S.; Franco, M. A.; Morais, F. G.; Machado, L. A. T.; Rizzo, L. V.; Cirino, G.; Pereira, A. G. C.; Ribeiro, P. D. S.; Barros, L. R. C.; et al. Evaluation of MODIS Dark Target AOD Product with 3 and 10 Km Resolution in Amazonia. *Atmosphere* **2022**, *13*, 1742. https://doi.org/10.3390/atmos13111742.
38. Palácios, R. D. S.; Morais, F. G.; Landulfo, E.; Franco, M. A. D. M.; Kuhnen, I. A.; Marques, J. B.; Nogueira, J. D. S.; Júnior, L. C. G. D. V.; Rodrigues, T. R.; Romera, K. S.; et al. Long Term Analysis of Optical and Radiative Properties of Aerosols in the Amazon Basin. *Aerosol Air Qual. Res.* **2020**, *20*, 139–154. https://doi.org/10.4209/aaqr.2019.04.0189.
39. Artaxo, P.; Gatti, L. V.; Leal, A. M. C.; Longo, K. M.; Freitas, S. R. D.; Lara, L. L.; Pauliquevis, T. M.; Procópio, A. S.; Rizzo, L. V. Atmospheric Chemistry in Amazonia: The forest and the biomass burning emissions controlling the composition of the Amazonian atmosphere. *Acta Amaz.* **2005**, *35*, 185–196. https://doi.org/10.1590/S0044-59672005000200008.
40. Nascimento, G. C.; Senna, M. C. A. The Influence of El Niño and La Niña Events in the Evaluation of the Fire Risk in Pará. *Anuário Inst. Geociências* **2020**, *43*. https://doi.org/10.11137/2020_4_189_201.
41. Barbosa, M. L. F.; Delgado, R. C.; Forsad De Andrade, C.; Teodoro, P. E.; Silva Junior, C. A.; Wanderley, H. S.; Capristo-Silva, G. F. Recent Trends in the Fire Dynamics in Brazilian Legal Amazon: Interaction between the ENSO Phenomenon, Climate and Land Use. *Environ. Dev.* **2021**, 39, 100648. https://doi.org/10.1016/j.envdev.2021.100648.
42. Silva Júnior, L. A. S.; Delgado, R. C.; Pereira, M. G.; Teodoro, P. E.; Da Silva Junior, C. A. Fire Dynamics in Extreme Climatic Events in Western Amazon. *Environ. Dev.* **2019**, *32*, 100450. https://doi.org/10.1016/j.envdev.2019.06.005.
43. Foley, J. A.; Botta, A.; Coe, M. T.; Costa, M. H. El Niño-Southern Oscillation and the Climate, Ecosystems and Rivers of Amazonia: IMPACT OF ENSO ON AMAZONIAN ECOSYSTEMS AND RIVERS. *Glob. Biogeochem. Cycles* **2002**, *16*, 79-1-79–20. https://doi.org/10.1029/2002GB001872.
44. Withey, K.; Berenguer, E.; Palmeira, A. F.; Espírito-Santo, F. D. B.; Lennox, G. D.; Silva, C. V. J.; Aragão, L. E. O. C.; Ferreira, J.; França, F.; Malhi, Y.; et al. Quantifying Immediate Carbon Emissions from El Niño-Mediated Wildfires in Humid Tropical Forests. *Philos. Trans. R. Soc. B Biol. Sci.* **2018**, *373*, 20170312. https://doi.org/10.1098/rstb.2017.0312.
45. Sousa, A. M. L.; Rocha, E. J. P. D.; Vitorino, M. I.; Souza, P. J. O. P.; Botelho, M. N. Spatio-Temporal Variability of Precipitation in the Amazon during Enso Events. *Rev. Bras. Geogr. Física* **2015**, *8*, 13-24. https://doi.org/10.13140/RG.2.1.4123.2401.
46. Souza, A. D.; Cavazzana, G. H.; Santos, D. A. D. S.; Abreu, M. C.; Fernandes, W. A.; Aristone, F. Relationship Between Aerosol Optical Depth And Precipitation Considering The Relative Humidity As An Influence Factor. *GEOgraphia* **2021**, *23*. https://doi.org/10.22409/GEOgraphia2021.v23i51.a27224.